ATOMIC-LAYER-DEPOSITED ALUMINUM OXIDE FOR THE SURFACE PASSIVATION OF HIGH-EFFICIENCY SILICON SOLAR CELLS

Jan Schmidt,[1] Agnes Merkle,[1] B. Hoex,[2] M.C.M. van de Sanden,[2] W.M.M. Kessels,[2] and Rolf Brendel[1]
[1]Institut für Solarenergieforschung Hameln (ISFH), Am Ohrberg 1, 31860 Emmerthal, Germany
[2]Department of Applied Physics, Eindhoven University of Technology, 5600 MB Eindhoven, The Netherlands

ABSTRACT

We present independently confirmed efficiencies above 20% for PERC-type solar cells with the point-contacted rear being either passivated by atomic-layer-deposited Al_2O_3 or by stacks consisting of an ultrathin Al_2O_3 film and a thicker PECVD-SiO_x layer. Internal quantum efficiency measurements reveal that the effective rear surface recombination velocities of the single-layer Al_2O_3-passivated cells are comparable to those measured on reference cells passivated by an aluminum-annealed thermal SiO_2, while those of the Al_2O_3/SiO_x-passivated cells are even lower. Very low effective rear surface recombination velocities of only 70 cm/s are reported for the Al_2O_3/SiO_x stacks, including metalized areas on the cell rear.

INTRODUCTION

In high-efficiency laboratory silicon solar cells [1,2], surface recombination is very effectively suppressed by means of silicon dioxide (SiO_2) grown in a high-temperature (≥ 900 °C) oxidation process. Very low surface recombination velocities (SRVs) are in particular realized at the lightly doped rear surface, where the combination of a thermally grown SiO_2 layer with an evaporated film of Al give – after an additional annealing treatment at ~400°C (the so-called 'alneal') – SRVs below 20 cm/s on un-metallized low-resistivity (~1 Ωcm) *p*-type silicon wafers [3]. In addition, the SiO_2/Al stack at the cell rear acts as an excellent reflector for near-bandgap photons, significantly improving the light trapping properties and hence the short-circuit current of the cell. One of the main reasons why high-temperature oxidation has not been implemented into the majority of industrial cell processes up to now is the high sensitivity of the silicon bulk lifetime to high-temperature processes. In particular in the case of multi-crystalline silicon wafers, thermal processes above 900°C typically lead to a significant degradation of the bulk lifetime [4]. Hence, low-temperature surface passivation alternatives are required for future industrial high-efficiency silicon solar cells, which should have comparable properties as the alnealed SiO_2.

LOW-TEMPERATURE SURFACE PASSIVATION

One intensively investigated low-temperature surface passivation alternative to thermal oxide is silicon nitride (SiN_x) grown by plasma-enhanced chemical vapor deposition (PECVD) at ~400°C, which has proven to give comparably low SRVs as thermal SiO_2 on low-resistivity *p*-type silicon [5,6]. However, when applied to the rear of PERC (Passivated Emitter and Rear Cell)-type solar cells the short-circuit current density is strongly reduced compared to the SiO_2-passivated cell rear [7]. This effect has been attributed to the large density of fixed positive charges within the SiN_x layer, inducing an inversion layer in the crystalline silicon underneath the SiN_x. The coupling of this inversion layer to the base contact leads to a significant loss in the short-circuit current density. This detrimental effect is known as 'parasitic shunting' [8]. Another alternative low-temperature passivation scheme resulting in comparable SRVs as alnealed SiO_2 is intrinsic hydrogenated amorphous silicon (a-Si) deposited by PECVD in the temperature range between 200 and 250°C [9]. Despite the fact that no parasitic shunting occurs in the case of an a-Si passivated cell rear, new problems arise from the high sensitivity of the a-Si passivation to thermal processes.

ATOMIC-LAYER-DEPOSITED Al_2O_3

Recently, it was shown that thin films of aluminum oxide (Al_2O_3) grown by atomic layer deposition (ALD) provide an excellent level of surface passivation on low-resistivity *p*- and *n*-type silicon wafers [10,11]. Figure 1 shows a comparison of the injection-dependent effective SRVs measured on 1-2 Ωcm *p*-type silicon wafers passivated by (i) SiN_x deposited by remote-PECVD [12], (ii) intrinsic a-Si deposited in a parallel-plate PECVD reactor [9], and (iii) Al_2O_3 deposited by means of plasma-assisted ALD [13]. The measurements are shown in the injection range between 10^{12} and 10^{15} cm^{-3}, which is the most relevant range for the rear of one-sun silicon solar cells. Within this injection range it becomes obvious from Fig. 1 that the Al_2O_3 passivation outperforms the well-optimized SiN_x as well as the a-Si passivation. Importantly, the Al_2O_3 passivation results in a very weak injection level dependence in the injection range between 10^{12} and 10^{15} cm^{-3}, and the effective SRV stays well below 10 cm/s even at low injection densities < 10^{13} cm^{-3}. The strong injection level dependence of the effective SRV measured on SiN_x-passivated *p*-Si surfaces can be attributed to recombination within the space charge region induced by the high fixed positive charge density within the SiN_x layer [6].

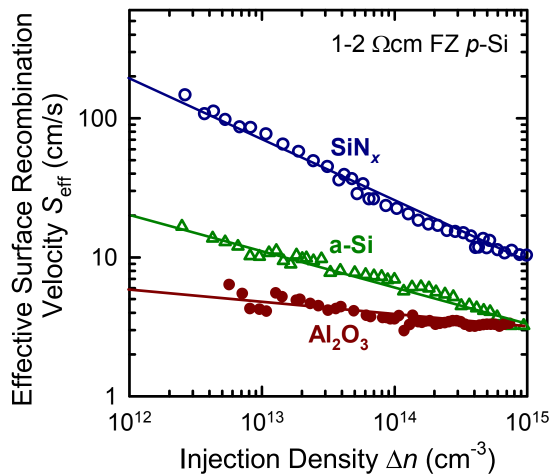

Fig. 1. Comparison of the injection-dependent effective SRVs $S_{eff}(\Delta n)$ measured on 1-2 Ωcm *p*-type silicon wafers passivated by (i) SiN_x deposited by remote-PECVD [14], (ii) intrinsic a-Si deposited in a parallel-plate PECVD reactor [9], and (iii) Al_2O_3 deposited by means of plasma-assisted ALD [13].

Figure 2 shows the measured effective SRV as a function of the Corona charge density deposited onto dielectric passivation layers of SiN_x and Al_2O_3. In the flatband case when the deposited Corona charge density equals the fixed charge density within the dielectric layer, the recombination rate shows a maximum. From this maximum the charge density within the layer can be deduced. As can be seen from Fig. 2, the fixed charge density within the SiN_x layer is positive and amounts to Q_f = $+2\times10^{12}$ elementary charges/cm^2, whereas the fixed charge density within the Al_2O_3 layer is negative and amounts to $Q_f = -1.3\text{x}10^{13}$ cm^{-2}. The fixed negative charge density within the Al_2O_3 layer induces an accumulation layer at the *p*-type silicon surface in contrast to the SiN_x layer inducing and inversion layer. As a consequence, the Al_2O_3 provides a very effective field-effect passivation without the additional contribution of recombination in the space charge region, which is the dominant recombination channel in the case of the SiN_x passivation of *p*-type silicon surfaces at low injection densities [6]. In addition, due to the formation of an accumulation layer instead of an inversion layer at the *p*-type silicon surface, the above-mentioned parasitic shunting effect at the solar cell rear is not expected for an Al_2O_3-rear-passivated cell. In combination with its very high transparency for near-bandgap photons, ALD-deposited Al_2O_3 should hence be an optimal choice for a dielectric layer at the silicon solar cell rear. In this contribution, we present first results of PERC-type solar cells with Al_2O_3-passivated rear surface, demonstrating the large potential of atomic-layer-deposited Al_2O_3 films for future high-efficiency silicon solar cells.

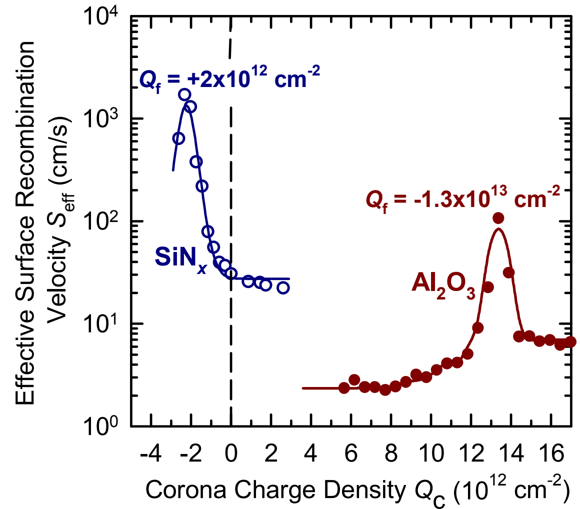

Fig. 2. Measured effective SRV S_{eff} as a function of the Corona charge density Q_C deposited onto dielectric passivation layers of SiN_x and Al_2O_3.

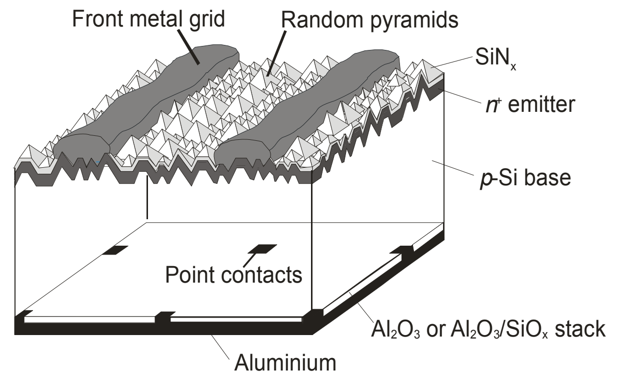

Fig. 3. PERC-type solar cell structure used to demonstrate the applicability of an Al_2O_3 rear surface passivation to high-efficiency solar cells.

ALD-PASSIVATED SOLAR CELLS

Figure 3 shows the PERC-type solar cell structure used in this study to demonstrate the applicability of Al_2O_3 rear surface passivation to high-efficiency silicon solar cells and Fig. 4 shows the corresponding process flow diagram. As starting material used is (100)-oriented boron-doped float-zone (FZ) silicon with a thickness of 310 µm and a resistivity of 0.5 Ωcm. After damage etching of ~10 µm/side and wet chemical cleaning, an SiO_2 layer is grown on both wafer surfaces in a wet oxidation process at 1000°C. Subsequently, 2×2 cm^2 diffusion windows are photolithographically opened on one wafer side and the silicon surface within the windows is textured with random pyramids in a KOH/isopropanol solution. A single-step phosphorus emitter is diffused from a $POCl_3$ source, resulting in an n^+-emitter with a sheet resistance of

Table 1: One-sun parameters measured under standard testing conditions of 290 µm thick PERC-type silicon solar cells with three different rear surface passivations: (i) thermal SiO_2 (220 nm), (ii) ALD-Al_2O_3 (130 nm) and (iii) ALD-Al_2O_3(30 nm)/PECVD-SiO_x(200 nm). All cells were fabricated on 0.5-Ωcm FZ *p*-Si wafers. The aperture cell area is 4 cm^2.

Rear side	Cell ID	V_{oc} [mV]	J_{sc} [mA/cm^2]	*FF* [%]	η [%]
Thermal SiO_2 (220 nm)	7_1	656	38.9	80.3	20.5
	Average of 4	655±1	38.4±0.5	80.3±1.3	20.2±0.3
ALD-Al_2O_3 (130 nm)	3_3	655	38.7	78.9	20.0*
	Average of 4	656±2	38.6±0.1	79.4±1.4	20.0±0.4
ALD-Al_2O_3 (30 nm)/ PECVD-SiO_x (200 nm)	2_4	660	39.0	80.1	20.6*
	Average of 8	657±2	38.6±0.3	80.4±1.1	20.4±0.4

*Calibrated measurement at Fraunhofer ISE CalLab.

100 Ω/square, and the phosphorus glass is removed by a short HF dip. At this point of the process, the cell batch is split up into three batches, of which each one receives a different rear surface passivation: (i) one batch of cells keeps the thermally grown SiO_2, (ii) the second one is coated by a 130 nm Al_2O_3 film and (iii) the third batch is passivated by a stack consisting of a 30 nm Al_2O_3 layer and a 200 nm thick PECVD-SiO_x layer deposited in a Plasmalab 80+ parallel-plate reactor (Oxford Instruments) at 425°C. The Al_2O_3 films are deposited by plasma-assisted ALD in a commercial ALD reactor (FlexAL^{TM}, Oxford Instruments) at a deposition temperature of 200°C [15]. The plasma-assisted ALD Al_2O_3 process is split up into two self-limiting reactions consisting of a tri-methyl-aluminum [$Al(CH_3)_3$] exposure and an O_2 plasma. The subsequent annealing step as applied in the study of Hoex et al. [11] is omitted in this case as adequate post-deposition annealing steps are already present in the process flow shown in Fig. 4. The SiO_x layer is deposited in a continuous PECVD process using silane (SiH_4) and di-nitrogen oxide (N_2O) as process gases. The remaining process steps are identical for all three cell batches. Using photolithography point contact openings are etched into the dielectric layers at the rear. A photolithography mask resulting in a point contact pitch of 2 mm and a metallization fraction of 4% is used. 20 µm of Aluminum is evaporated on the entire cell rear using electron-beam evaporation. A tunnel oxidation of the n^+-emitter is performed at 500°C for 10 min, resulting in an ~1.5 nm thick oxide layer [16]. The 20 µm thick Al front metal grid is then evaporated through a shadow mask onto the tunnel oxide. Finally, a surface-passivating SiN_x antireflection coating is deposited onto the front of the PERC solar cell by remote-PECVD at 300°C [5]. Before characterization all solar cells receive an additional 1-min 300°C anneal in air, which slightly improves the fill factor and the open-circuit voltage. The aperture area of all solar cells fabricated in this study is 4 cm^2 and the entire front metallization, including the busbar, is within the active cell area.

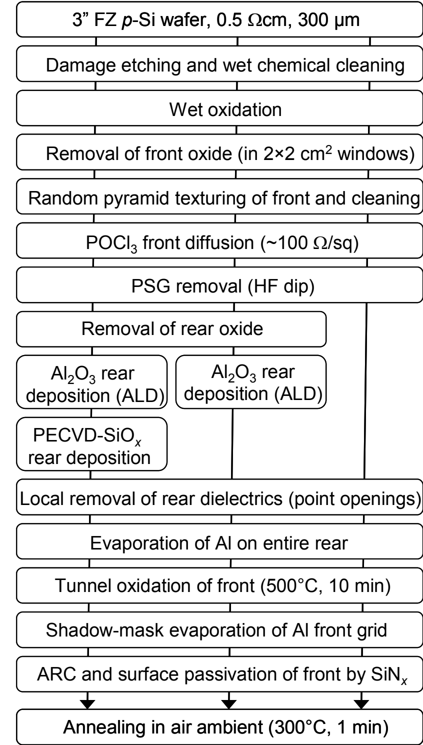

Fig. 4. Process flow diagram for the PERC-type solar cells fabricated in this study.

Table 1 summarizes the one-sun parameters of the processed PERC-type solar cells featuring different rear surface passivation schemes, as measured under standard testing conditions (25°C, 100 mW/cm^2, AM 1.5 G). The results marked with an asterisk were independently confirmed at Fraunhofer ISE CalLab. The best reference

Table 2: Effective rear surface recombination velocity S_r and internal rear reflectance R_r extracted from the *IQE* measurements shown in Fig. 5.

Rear side	Rear surface recombination velocity S_r [cm/s]	Internal rear reflectance R_r [%]
Thermal SiO_2 (220 nm)	90 ± 20	91 ± 1
Al_2O_3 (130 nm)	90 ± 20	90 ± 1
Al_2O_3(30 nm)/SiO_x(200 nm)	70 ± 20	91 ± 1

solar cell with alnealed SiO_2 rear surface passivation is characterized by an efficiency of η = 20.5%, an open-circuit voltage of V_{oc} = 656 mV and a short-circuit current density of J_{sc} = 38.9 mA/cm^2. The analysis of the internal quantum efficiency (*IQE*) shows that the V_{oc} is limited by the front emitter. The average values of all 4 cells with SiO_2 rear passivation show only a very small scatter, demonstrating the high reproducibility of the process. The average parameters of the cells with Al_2O_3, Al_2O_3/SiO_x and SiO_2 rear passivation agree within the scatter ranges. In particular it is noticeable that the J_{sc} of the cells with Al_2O_3 and Al_2O_3/SiO_x rear surface passivation is not reduced compared to the SiO_2-passivated cells. In the case of high-positive-charge dielectrics, such as SiN_x with fixed positive charge densities >10^{12} cm^{-2}, it was reported that J_{sc} is reduced by 1-2 mA/cm^2 compared to the thermal SiO_2 reference, due to the above-described parasitic shunting effect [7,8]. This effect is not expected in the case of Al_2O_3 as it is a negative-charge-dielectric inducing an accumulation layer. The cell results summarized in Table 1 confirm the expected non-existence of the parasitic shunting for Al_2O_3-passivated as well as for Al_2O_3/SiO_x-passivated rear surfaces. The best cell of the entire batch is obtained for the Al_2O_3/SiO_x-passivated cell, resulting in an independently confirmed efficiency of η = 20.6%, a V_{oc} of 660 mV and a J_{sc} of 39.0 mA/cm^2.

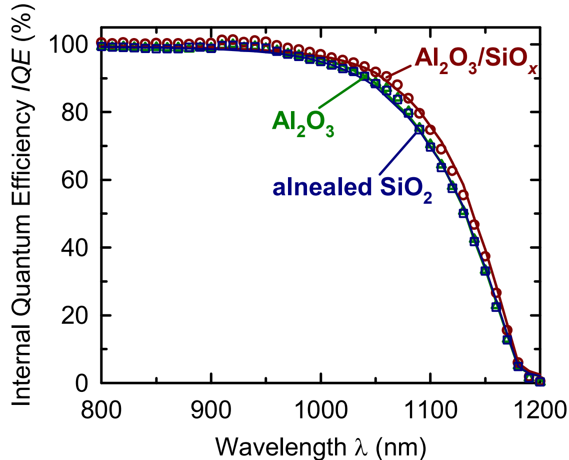

Fig. 5. Measured internal quantum efficiency *IQE* as a function of wavelength λ (symbols) for solar cells with three different rear surface passivations: (i) thermal SiO_2 (220 nm), (ii) ALD-Al_2O_3 (130 nm) and (iii) ALD-Al_2O_3(30 nm)/PECVD-SiO_x(200 nm). The lines show the fitted *IQE*(λ) curves. All measurements were taken with a white bias light intensity of ~0.3 suns.

It is not possible to quantify the exact rear surface passivation quality from comparison of the cell parameters given in Table 1, as these solar cells are largely limited by recombination losses in the front emitter. Hence, we analyze the *IQE* in the wavelength range 800-1200 nm to determine the rear SRVs of the different rear surface passivation schemes. The symbols in Fig. 5 show the *IQE* as a function of wavelength λ of PERC cells with the three different rear passivation schemes, measured at a fixed bias light intensity of 0.3 suns. The solid lines in Fig. 5 show the fits to the measured data. To model the *IQE*(λ) dependence we use the software LASSIE [17,18], which combines the extended *IQE* evaluation by Basore [19] with the improved optical model developed by Brendel [20]. The bulk lifetime is assumed to be limited by Auger recombination, resulting in a bulk diffusion length of L_b = 1500 µm for the 0.5 Ωcm *p*-type silicon material used in this work [21]. As we assume the intrinsic upper limit for the bulk lifetime, the SRVs determined from the *IQE* analysis are upper limits as well. Table 2 summarizes the rear SRVs S_r and the internal rear reflectances R_r extracted from the *IQE* analysis. All three rear structures are equally effective reflectors for near-bandgap photons (R_r = 91%). The rear SRV of the reference cell with alnealed SiO_2 amounts to S_r = (90 ± 20) cm/s. The extracted S_r for the cell with single-layer Al_2O_3 rear passivation is the same as for the SiO_2-passivated reference cell, showing that ALD-deposited Al_2O_3 performs as good as aluminum-annealed high-temperature-grown SiO_2. A further reduction in the S_r is obtained for the Al_2O_3/SiO_x stack, resulting in an S_r of only (70 ± 20) cm/s, which we attribute to the hydrogenation of interface states at the Al_2O_3/Si interface during deposition of the hydrogen-rich SiO_x layer.

The effective SRV of a point-contacted rear is given by Fischer's equation:[18]

$$S_r = \frac{D_n}{W}\left[\begin{array}{c}\frac{p}{2W\sqrt{\pi f}}\arctan\left(\frac{2W}{p}\sqrt{\frac{\pi}{f}}\right)\\ -\exp\left(-\frac{W}{p}\right)+\frac{D_n}{fWS_{met}}\end{array}\right]^{-1}+\frac{S_{pass}}{1-f}, \quad (1)$$

where D_n is the electron diffusion coefficient, W the wafer thickness, p the contact pitch, f the metallization fraction and S_{met} and S_{pass} are the SRVs on the metallized and on the passivated areas of the rear. According to Eqn. (1) the minimum SRV $S_{r.min}$ for a point-contact rear with perfect passivation in the non-metallized area (i.e., $S_{pass} = 0$) is given by the first summand on the right-hand side of Eqn. (1). For our cell structure we determine $S_{r.min}$ = 73 cm/s (D_n = 23 cm^2/s, W = 290 µm, p = 2000 µm, f = 4%, $S_{met} \geq 10^5$ cm/s), clearly demonstrating that in the case of the Al_2O_3/SiO_x stack, recombination in the passivated area of the cell rear can be completely neglected. Note that, although a slightly better passivation is obtained in the case of the Al_2O_3/SiO_x stacks, the rear SRV of the single-layer Al_2O_3-passivated cells is also mainly determined by recombination at the metal contacts. The *IQE* results clearly prove that atomic-layer-deposited Al_2O_3 is a very effective new dielectric passivation layer for high-efficiency silicon solar cells.

CONCLUSIONS

The excellent silicon surface passivation by atomic-layer-deposited Al_2O_3, which had up to now only been demonstrated by lifetime measurements, has successfully been transferred to the device level for the first time.

In addition to the outstanding surface passivation provided by ALD-deposited Al_2O_3, the deposition process itself is also beneficial from an application point of view. In contrast to the conventionally applied PECVD, ALD consists of two self-limiting half-reactions, which implies several important advantages: (i) ALD gives highly conformal coatings, which allows to deposit and passivate e.g. deep trenches or even pores in silicon, (ii) pin-hole and particle-free deposition is achieved, (iii) as ALD is a self-limiting process uniform films can be deposited over large areas with mono-layer growth control, and (iv) very low impurity concentrations of deposited films and hence very high film quality is achieved. The main disadvantage of ALD for photovoltaic applications is its relatively low deposition rate. However, as shown in this study, this disadvantage can be overcome by depositing ultrathin (2-30 nm) ALD-Al_2O_3 films and capping them with a thicker film of e.g. PECVD-SiO_x. Apart of the advantageous optical properties of these stacks, we have demonstrated that the passivation quality of such ALD-Al_2O_3/PECVD-SiO_x stacks can even be superior to that of single layers of Al_2O_3, which we attribute to the hydrogenation of interface states at the Al_2O_3/Si interface during deposition of the hydrogen-rich SiO_x layer. The same beneficial effect can be observed for other hydrogen-rich PECVD-deposited films, such as SiN_x or SiC_x. Combination of ALD and PECVD might hence be a key technology for future industrial high-efficiency solar cells.

Acknowledgments

The authors thank all members of the photovoltaic department at ISFH for their contributions to this work and W. Keuning (Eindhoven University of Technology) for carrying out the Al_2O_3 depositions. We gratefully acknowledge the financial support provided by the German State of Lower Saxony and the Netherlands Technology Foundation STW.

REFERENCES

[1] A. Aberle, W. Warta, J. Knobloch, B. Voß, *Proc. 21st IEEE PVSC* (1990), p. 233.

[2] J. Zhao, A. Wang, M.A. Green, *Prog. Photovolt.* **7,** 471 (1999).

[3] M.J. Kerr, A. Cuevas, *Sem. Sci. Techn.* **17**, 35 (2001).

[4] M.J. Stocks, A. Cuevas, A.W. Blakers, *Proc. 14th EUPVSEC*, Barcelona, Spain (1997), p. 770.

[5] T. Lauinger, J. Schmidt, A.G. Aberle, R. Hezel, *Appl. Phys. Lett.* **68**, 1232 (1996).

[6] J. Schmidt, J.D. Moschner, J. Henze, S. Dauwe, R. Hezel, *Proc. 19th EUPVSEC*, Paris, France (2004), p. 391.

[7] S. Dauwe, L. Mittelstädt, A. Metz, J. Schmidt, R. Hezel, *Proc. 3rd WCPEC*, Osaka, Japan (2003), p. 1395.

[8] S. Dauwe, L. Mittelstädt, A. Metz, R. Hezel, *Progr. Photovolt.* **10**, 271 (2002).

[9] S. Dauwe, J. Schmidt, R. Hezel, *Proc. 29th IEEE PVSEC*, New Orleans, USA (2002), p. 1246.

[10] G. Agostinelli, A. Delabie, P. Vitanov, Z. Alexieva, H.F.W. Dekkers, S. De Wolf, G. Beaucarne, *Sol. En. Mat. Sol. Cells* **90**, 3438 (2006).

[11] B. Hoex, S.B.S. Heil, E. Langereis, M.C.M. van de Sanden, W.M.M. Kessels, *Appl. Phys. Lett.* **89**, 042112 (2006).

[12] S. Dauwe, *Low-temperature rear surface passivation of crystalline silicon solar cells*, Ph.D. thesis, ISFH, University of Hanover, Germany, 2003.

[13] B. Hoex, J. Schmidt, P. Pohl, M.C.M. van de Sanden, W.M.M. Kessels, *J. Appl. Phys.*, in press.

[14] S. Dauwe, *Low-temperature rear surface passivation of crystalline silicon solar cells*, Ph.D. thesis, ISFH, University of Hanover, Germany, 2003.

[15] J.L. van Hemmen, S.B.S. Heil, J. Klootwijk, F. Roozeboom, C.J. Hodson, M.C.M. van de Sanden, W.M.M. Kessels, *J. Electrochem. Soc.* **154**, G165 (2007).

[16] R. Hezel, A. Metz, *Proc. 16th EUPVSEC*, Glasgow, UK (2000), p. 1091.

[17] www.pv-tools.de

[18] B. Fischer, *Loss analysis of crystalline silicon solar cells using photoconductance and quantum efficiency measurements*, Ph.D. thesis, University of Konstanz, 2003.

[19] P.A. Basore, *Proc. 23rd IEEE PVSC* (1993), p. 147.

[20] R. Brendel, R. Plieninger, *Techn. Digest 9th International PVSEC*, Miyazaki, Japan (1996), p. 521.

[21] P.P. Altermatt, J. Schmidt, G. Heiser, A.G. Aberle, *J. Appl. Phys.* **82**, 4938 (1997).